

## Frustration driven magnetic states of A-site spinels probed by $\mu$ SR

G. M. Kalvius, Alexander Krimmel, O. Hartmann, F. J. Litterst, R. Wäppling, F. E. Wagner, Vladimir Tsurkan, Alois Loidl

### Angaben zur Veröffentlichung / Publication details:

Kalvius, G. M., Alexander Krimmel, O. Hartmann, F. J. Litterst, R. Wäppling, F. E. Wagner, Vladimir Tsurkan, and Alois Loidl. 2010. "Frustration driven magnetic states of A-site spinels probed by  $\mu$ SR." *The European Physical Journal B* 77 (1): 87–100.  
<https://doi.org/10.1140/epjb/e2010-00262-7>.



# Frustration driven magnetic states of A-site spinels probed by $\mu$ SR

G.M. Kalvius<sup>1</sup>, A. Krimmel<sup>2</sup>, O. Hartmann<sup>3</sup>, F.J. Litterst<sup>4</sup>, R. Wäppling<sup>3</sup>, F.E. Wagner<sup>1</sup>, V. Tsurkan<sup>2,5,a</sup>, and A. Loidl<sup>2</sup>

<sup>1</sup> Physics Department, Technische Universität München, 85747 Garching, Germany

<sup>2</sup> Experimental Physics V, Center for Electronic Correlations and Magnetism, Universität Augsburg, 86159 Augsburg, Germany

<sup>3</sup> Department of Physics and Astronomy, Uppsala University, 75120 Uppsala, Sweden

<sup>4</sup> IPKM, Technische Universität Braunschweig, 38106 Braunschweig, Germany

<sup>5</sup> Institute of Applied Physics, Academy of Sciences, 2028 Chisinau, Republic of Moldova

**Abstract.** The normal A-site spinels  $\text{MnAl}_2\text{O}_4$ ,  $\text{FeAl}_2\text{O}_4$ ,  $\text{CoAl}_2\text{O}_4$ , as well as related mixed ( $\text{Mn}_{0.5}\text{Fe}_{0.5}\text{Al}_2\text{O}_4$ ) and partially inverted ( $\text{Fe}_{1.4}\text{Al}_{1.6}\text{O}_4$ ) spinels have been studied by  $\mu$ SR. The magnetic ions are subject to magnetic frustration by competing interactions. In all materials and at all temperatures the  $\mu$ SR spectra consist of two signals suggesting a bimodal distribution of the fluctuation rates of magnetic moments. A characteristic temperature  $T_M$  is found in each compound, representing either a magnetic phase transition into a long-range ordered state ( $\text{MnAl}_2\text{O}_4$ ,  $\text{Fe}_{1.4}\text{Al}_{1.6}\text{O}_4$ ) or the formation of a spin liquid phase ( $\text{FeAl}_2\text{O}_4$ ,  $\text{CoAl}_2\text{O}_4$ ,  $\text{Mn}_{0.5}\text{Fe}_{0.5}\text{Al}_2\text{O}_4$ ). The magnetic ground state of  $\text{MnAl}_2\text{O}_4$  shows coexistence of antiferromagnetic and spin liquid phases. In  $\text{FeAl}_2\text{O}_4$  and  $\text{CoAl}_2\text{O}_4$  long-range order is suppressed altogether, the ground state can be characterized as a fast relaxing spin liquid coexisting with a small fraction of paramagnetic spins. The partial replacement of Mn by Fe in  $\text{Mn}_{0.5}\text{Fe}_{0.5}\text{Al}_2\text{O}_4$  prevents long-range order and leads to a spin liquid state in the low temperature limit. The partial occupancy of B-sites by magnetic ions in  $\text{Fe}_{1.4}\text{Al}_{1.6}\text{O}_4$  strengthens the exchange coupling, allowing the formation of long-range magnetic order at a rather high temperature ( $\sim 100$  K). Magnetic phase diagrams are presented demonstrating that for the studied compounds the magnetic properties are determined by the degree of frustration.

## 1 Introduction

Spinel compounds comprise an important class of compounds, including minerals (e.g.  $\text{FeAl}_2\text{O}_4$  is known as Hercynite) which exhibit a wide variety of magnetic properties. Their stoichiometry is described by the formula  $(\text{A})[\text{B}_2]\text{O}_4$ . The oxygen ions form a cubic-close packed sublattice which tends to be slightly distorted in real crystals. Divalent cations (A) are located at the tetrahedrally oxygen coordinated A-sites, trivalent cations [B] occupy the octahedrally coordinated B-sites. The distortion of the oxygen sublattice causes a trigonal distortion of the B-site octahedron but does not influence the A-site. Another deviation from an ideal spinel is inversion, meaning a site exchange between A-site and B-site ions. In well prepared samples one commonly has inversion of a few percent, but fully (100%) inverted spinels of stoichiometry  $(\text{A})[\text{AB}]\text{O}_4$  also exist.

One distinguishes between A-site and B-site spinels depending on which site is occupied by the magnetic ion. The latter case is most common and also most thoroughly

studied. The magnetic B-site lattice is of the pyrochlore type resulting in geometric magnetic frustration. A typical example is  $\text{ZnFe}_2\text{O}_4$  (see [1] and references therein). Numerous theoretical treatments of B-site spinels exist, including the fundamental work by Anderson [2].

For the A-site spinels much less information is available. There the magnetic ions form a diamond sublattice which consists of two interpenetrating fcc-lattices. In itself, the diamond lattice is not geometrically frustrated. The situation with antiferromagnetic interactions has been treated theoretically rather recently [3]. It was found that substantial magnetic frustration exists affecting both spin and orbital degrees of freedom which arises primarily from the presence of multiple exchange interactions [4,5]. In particular it is shown that the parameter which mainly controls the nature of the magnetic ground state is the ratio of next-nearest to nearest neighbor exchange.

The exchange paths of the A-site spinels are complex [6]. Direct (A-A) exchange between the four nearest neighbors is ineffective due to their large separation ( $\sim 3.4$  Å). These four ions are rather coupled by

<sup>a</sup> e-mail: vladimir.tsurkan@physik.uni-augsburg.de

six indirect A-O-Al-O-A exchange routes  $J$  featuring  $90^\circ$  O-Al-O bonds. The twelve next nearest neighbors interact via similar exchange routes  $J'$ . Furthermore, one needs to take into account the exchange  $J''$  between the twelve next next nearest neighbors which include  $180^\circ$  O-Al-O bonds. All three couplings are antiferromagnetic and tri-angulantly coordinated. Well known A-site spinels, other than those treated here, are the sulfur spinels  $\text{FeSc}_2\text{S}_4$  and  $\text{MnSc}_2\text{S}_4$  [4,7,8], with the iron compound being a famous example for the formation of a spin-orbital liquid magnetic ground state. A brief  $\mu\text{SR}$  study of those materials has been published [9]. A theoretical study on quantum criticality [10] shows that disordered orbital degrees of freedom (spin orbital singlet) further suppresses spin order. In case of orbital order one might expect spin order or a spiral spin liquid phase. The experimental data cited above point to a spin liquid phase.

The study of frustration effects in magnetic systems is of substantial current interest. In general, magnetic frustration suppresses long-range order, in particular simple collinear antiferromagnetic spin arrangements. Rather often exotic magnetic ground states are formed [11,12] such as long wavelength spiral order or various types of short-range ordered states. Another typical effect of frustration is the presence of distinct spin fluctuations. As shown in particular by  $\mu\text{SR}$  [13–15] these spin fluctuations, which often are of rather low frequency (in the range of MHz), tend to persist in the limit  $T \rightarrow 0$ . This unusual, but characteristic feature is independent of the source of frustration as seen, for example, from the works cited above.

The  $3d$  magnetic ions of the three  $\text{AAl}_2\text{O}_4$  spinels under investigation differ in their spin properties. The tetrahedral crystal field at the  $A$ -site splits the  $3d$  manifold into a lower doublet and an excited triplet.  $\text{Mn}^{2+}$  ( $3d^5$ ) has a half filled  $3d$  shell with  $S = 5/2$  and no orbital moment.  $\text{Co}^{2+}$  ( $3d^7$ ) has  $S = 3/2$  and weak spin-orbit coupling.  $\text{Fe}^{2+}$  ( $3d^6$ ) has  $S = 2$  and is weakly Jahn-Teller active. The bulk magnetic properties of the pure compounds  $\text{AAl}_2\text{O}_4$  ( $A = \text{Mn}, \text{Fe}, \text{Co}$ ) are well documented [16,17].

For the partially inverted spinel  $\text{Fe}_{1.4}\text{Al}_{1.6}\text{O}_4$  and the mixed spinel  $\text{Mn}_{0.5}\text{Fe}_{0.5}\text{Al}_2\text{O}_4$  included in this work, such information is not available. They are here studied for the first time. Some bulk magnetization data taken in the context of this work are presented in addition to the  $\mu\text{SR}$  results.

$\text{MnAl}_2\text{O}_4$ ,  $\text{FeAl}_2\text{O}_4$ ,  $\text{CoAl}_2\text{O}_4$  show Curie-Weiss behavior at high temperatures. The Curie-Weiss temperatures, determined from the high temperature slopes of the inverse susceptibilities, were  $\Theta_{\text{CW}} = -143\text{ K}$  (Mn),  $-130\text{ K}$  (Fe),  $-104\text{ K}$  (Co). They roughly scale with the spin moments. Their magnitudes stress that the antiferromagnetic exchange is strong.

In  $\text{MnAl}_2\text{O}_4$  neutron diffraction sees below  $T_{\text{N}} = 40\text{ K}$  the magnetic Bragg pattern of simple collinear antiferromagnetic order [5]. In addition, a sizable diffuse magnetic scattering signal is observed below  $T_{\text{N}}$  indicating coexisting paramagnetic spins. The temperature dependence of the ordered Mn magnetic moment has the shape of a Brillouin magnetization curve with a saturated moment

$\mu_{\text{ord}} = 3.7 \mu_{\text{B}}$ . This is to be compared with the pure spin moment  $\mu_{\text{spin}} = 5 \mu_{\text{B}}$  leading to the ratio of observed to expected moment  $\mu_{\text{ord}}/\mu_{\text{spin}} = 3.7/5 = 0.74$ .

In  $\text{FeAl}_2\text{O}_4$  and  $\text{CoAl}_2\text{O}_4$  magnetic Bragg peaks were not found down to  $2\text{ K}$ . Susceptibility measurements saw cusps at  $T_{\text{cusp}} = 11\text{ K}$  (Fe) and  $T_{\text{cusp}} = 5\text{ K}$  (Co). These anomalies are also visible as broad cusp-like maxima in the heat capacity. The susceptibilities below  $T_{\text{cusp}}$  show splitting of the field-cooled and zero-field cooled branches, suggesting spin-glass-like freezing. That notion is further supported by a liquid-like magnetic structure factor in neutron diffraction which indicates pure short-range correlations [17]. On the other side, heat capacity below  $T_{\text{cusp}}$  has a  $T^2$ -temperature dependence as observed in other frustrated magnets, and not the linear dependence expected for a spin glass. In the Jahn-Teller active Fe compound heat capacity data reveal that orbital degrees of freedom have to be taken into account as well [16].

The ratio  $f$  between the Curie-Weiss temperature reflecting the energy scale of the leading magnetic exchange, and the characteristic magnetic temperature  $T_{\text{M}}$  indicating the onset of spin order or spin freezing is commonly taken as a measure of frustration [11]. When using  $T_{\text{N}}$  for  $\text{MnAl}_2\text{O}_4$  and  $T_{\text{cusp}}$  for  $\text{CoAl}_2\text{O}_4$  and  $\text{FeAl}_2\text{O}_4$  as the characteristic temperatures  $T_{\text{M}}$  together with the values of  $\Theta_{\text{CW}}$  listed above, one obtains frustration parameters  $f = 3.6$  (Mn),  $11$  (Fe), and  $22$  (Co). Consistent with that result is that only the weakly frustrated  $\text{MnAl}_2\text{O}_4$  is capable of forming a long-range ordered magnetic state at low temperatures.

A single Mössbauer study on  $\text{FeAl}_2\text{O}_4$  has been published [18]. The majority of Fe-ions were in the  $2+$  state, as expected, but a weak signal from  $\text{Fe}^{3+}$ -ions was also present. An assignment of this trivalent portion was not possible. Below a critical temperature of  $13\text{ K}$  the spectra changed from a quadrupole doublet into a poorly resolved magnetic pattern which was interpreted as the signature of a spin-glass-like state. The mean hyperfine field vanishes rather suddenly at  $13\text{ K}$  as in a first order transition which remained unexplained. Unfortunately, the Mössbauer spectra of spin glasses are not sensitive to details of the spin frozen state like the interplay between static spin disorder and spin dynamics.

In the present work we explore the magnetic states of frustrated A-site spinels in view of the interplay between long-range ordered and short-range spin correlated states as function of frustration.  $\mu\text{SR}$  spectroscopy is a most powerful tool for such studies. Being a local magnetic probe (i.e. sensing magnetic properties predominantly over the range of a few lattice parameters) it contrasts and expands information obtained by bulk magnetic measurements and neutron diffraction. It possesses a high sensitivity to short-range spin disorder and to low frequency spin fluctuations, features often found in frustrated magnets. Especially the unique sensitivity of  $\mu\text{SR}$  to moment fluctuation rates in the MHz range allows the distinction between spin glass and spin liquid states. Furthermore, in case of coexistence of different magnetic states, the intensity of the related signals is directly proportional

(i.e. without any correcting factors, like the Debye-Waller Factor or saturation effects) to the volume fraction of those states. Powder samples suffice (and are even preferable) for most magnetic studies.

The selection of compounds to be studied allows to trace the differences in magnetic behavior between compounds having a spin only ( $\text{MnAl}_2\text{O}_4$ ), a spin-orbit coupled ( $\text{CoAl}_2\text{O}_4$ ) or a weakly Jahn-Teller active ( $\text{FeAl}_2\text{O}_4$ ) magnetic ion. In addition, in studying  $\text{Mn}_{0.5}\text{Fe}_{0.5}\text{Al}_2\text{O}_4$  we seek information on the effect of A-site disorder (substituting Fe in part for Mn) and by probing  $\text{Fe}_{1.4}\text{Al}_{1.6}\text{O}_4$ , or better  $(\text{Fe})[\text{Fe}:\text{Al}]_2\text{O}_4$ , on the influence of partial inversion with B-site disorder. The results will be compared with the recent theoretical treatments [3,10]. Some data on the pure  $\text{AAl}_2\text{O}_4$  compounds have previously been presented in a brief conference report [19].

## 2 Experimental

Polycrystalline samples were prepared by solid state reaction from high purity binary oxides in evacuated quartz ampoules. To get the smallest possible inversion, the synthesis must be carried out at the lowest allowable temperature which was found to be  $1000^\circ\text{C}$ . To assure homogeneity the samples were slowly ( $\sim 15^\circ/\text{h}$ ) cooled to room temperature. Sample purity was checked by powder X-ray diffraction. No foreign phase could be detected. For the  $\mu\text{SR}$  measurements a small amount of powder was pressed into a cylindrical tablet and mounted between sheets of thin aluminized Mylar tape on a fork-like sample holder in order to minimize foreign material around the sample. The sample thickness well exceeded the stopping distance for low energy muons.

The  $\mu\text{SR}$  experiments were conducted with surface muons between 2 K and 200 K using a He-flow cryostat. The sample position within the He gas flow ensured good thermal contact. Weak transverse field (TF), zero field (ZF) and longitudinal field (LF) measurements were carried out. In TF measurements an external magnetic field is applied perpendicular to the muon beam, in LF measurements, the field is oriented parallel to the beam. Care is taken to compensate at the sample position any stray fields from surrounding magnets or the earth field in case of ZF measurements. Typically a total of 5–6 million events were recorded per spectrum, corresponding to a measuring time of about 1 h. The time resolution was 1.25 ns and the initial dead time of the spectrometer amounted to about 5 ns. The VETO method [20] was enabled in order to suppress any signal from muons stopped in matter outside the sample (background signal). Indeed, as checked by TF data, no background signal existed in the present set of measurements.

## 3 Magnetic $\mu\text{SR}$ spectra

Details on the  $\mu\text{SR}$  technique can be found, for example, in [21–24]. Positive muons with their spins fully polarized along the beam direction are implanted into the

sample. They are quickly stopped at an interstitial lattice site keeping their spin polarization. Except in some very pure elemental metals or in simple binary alloys, the muons remain stationary at their stopping site at least up to some 100 K. The muons decay with a mean life time of  $\tau_\mu = 2.2 \mu\text{s}$  emitting a positron preferentially along the direction the muon spin is pointing. By placing two positron detectors along the beam line in front and behind the sample, respectively, one records the backward-forward asymmetry of positron count rates  $A(t)$  as function of the time  $t$  elapsed since the moment of muon implantation. Usually a time span of 3 to 4 mean muon life times is covered. A plot of  $A(t)$  vs.  $t$  constitutes the  $\mu\text{SR}$  spectrum which is generally described by

$$A(t) = A_0 G(t) \quad (1)$$

with  $A_0$  being the initial ( $t = 0$ ) asymmetry (typically around 0.2) and  $G(t)$  the muon spectral function describing the temporal evolution of the muon spin polarization due to the interaction with the magnetic field  $B_\mu$  at the muon site. If externally applied fields are not present, the source of  $B_\mu$  are for each atom surrounding the stopped muon its nuclear moment and its total moment of the atomic shell where a separation in spin and orbital contribution is not possible. The muon has no quadrupole moment and direct interactions with electric field gradients are absent.

The  $\mu\text{SR}$  spectra are analyzed by least squares fitting the appropriate spectral function  $G(t)$  to the measured spectrum  $A(t)$  given by equation (1). The parameters of  $G(t)$  are the physical quantities of interest and can be related rather directly to the static and dynamic properties of the magnetic spin system. For the derivation and the properties of the various spectral functions we refer the reader back to the literature cited above. However, in order to ease the understanding of the  $\mu\text{SR}$  spectra shown, we briefly discuss the functions  $G(t)$  appearing in this work.

### 3.1 Paramagnets

In ZF one observes an exponential decay of asymmetry which is described by:

$$G(t)_{par}^{ZF} = \exp(-\lambda t) \quad \text{with} \quad \lambda = \gamma_\mu^2 \langle B_\mu^2 \rangle \tau \quad (2)$$

where  $\gamma_\mu/2\pi = 135.54 \mu\text{s}^{-1}/\text{T}$  is the muon gyromagnetic ratio, and  $\langle B_\mu^2 \rangle$  the second moment of the distribution of the field at the muon site. One often uses the *rms* field  $B_{rms} = \sqrt{\langle B_\mu^2 \rangle}$ . Finally,  $1/\tau$  is the fluctuation rate of  $B_\mu$  and thus reflects the fluctuation of the moments which create  $B_\mu$ . It is important to note that in paramagnets the slowing down of fluctuations of the magnetic moments increases the muon spin relaxation rate  $\lambda$ . This emphasizes that one needs to distinguish between the muon spin relaxation rate  $\lambda$  which describes the loss of asymmetry in time and the fluctuation rate  $1/\tau$  which drives the muon spin relaxation process.

One commonly also performs TF measurements in the paramagnetic regime. The muons then carry out Larmor precession in the applied field leading to an oscillatory pattern:

$$G(t)_{par}^{TF} = \exp(-\lambda t) \cos(\omega_\mu t) \quad \text{with} \quad \omega_\mu = \gamma_\mu B_\mu. \quad (3)$$

The applied field  $B_{TF}$  weakly polarizes the paramagnetic spin ensemble. This has two consequences. First, the muon spin relaxation rate now contains an additional static contribution (inhomogeneous line broadening) caused, for example, by the demagnetizing field. This means that the rates  $\lambda$  in equations (2) and (3) are different under otherwise equal physical conditions [25]. Second, the magnitude of  $B_\mu$  is not exactly that of  $B_{TF}$ . This effect is known as the muon Knight shift.

In the present study we used, for reasons explained further below (Sect. 4), only very weak transverse fields ( $B_{TF} = 3$  mT). Then the above mentioned effects are negligible, and, in particular, the muon spin relaxation rates  $\lambda$  obtained by either TF or ZF measurements can be treated on the same footing. A muon Knight shift cannot be resolved.

### 3.2 Long-range ordered magnets

A spin precession pattern is observed in ZF whose form, for an isotropic powder sample, is:

$$G(t)_{lro}^{ZF} = (2/3) \exp(-\lambda_{trans} t) \cos(\omega_\mu t) + (1/3) \exp(-\lambda_{long} t). \quad (4)$$

The two terms arise from the usual approach to describe the isotropic average by assuming that in 2/3 of the cases the internal field is aligned perpendicular to the initial muon spin direction causing Larmor precession (transverse term) while in 1/3 of the cases the field is oriented parallel to the muon spins and thus does not induce spin precession (longitudinal term). The muon spin relaxation rates are different in the two terms. The longitudinal relaxation is caused exclusively by dynamics of the magnetic moments leading to  $\lambda_{long} = 2/(3\tau)$ . Note that here  $\lambda_{long} \propto 1/\tau$  while in paramagnets  $\lambda \propto \tau$ . The transverse relaxation originates from the static field distribution and also from spin dynamics. Usually the relation  $\lambda_{long} \ll \lambda_{trans}$  is fulfilled and one approximates  $\lambda_{trans} \approx \gamma_\mu B_{rms}$ . The spectrum of a long-range ordered magnet thus consists of a damped oscillatory pattern on top of an exponentially decaying line. The effective field causing the spin precession has in normal cases a temperature dependence close to that of the sublattice magnetization.

TF measurements are in general not very useful in ordered magnets. However, a weak  $B_{TF}$ , as used in the present work, is negligible compared to  $B_\mu$  created by the magnetic moments and the observed spectra are essentially the same as in ZF. In a magnet with ferromagnetic component a weak external field will not enter the bulk.

### 3.3 Spin glasses

In ZF the spectral response of an ideal spin glass is the Lorentzian Kubo-Toyabe pattern [26,27]. In the static limit, i.e. below the glass transition temperature  $T_G$ , it has the form:

$$G(t)_{SG}^{ZF} G(t) = (2/3)(1 - at) \exp(-at) + (1/3) \quad (5)$$

where  $a/\gamma_\mu$  is the half width at half maximum ( $B_{HWHM}$ ) of the field distribution. The muon spin polarization decays exponentially at the beginning, passes through a minimum, and after recovering to 1/3, remains time independent. The origin of the ‘1/3-signal’ is the same as in equation (4). Passing  $T_G$  from the low temperature side, spin dynamics sets in. The resulting dynamic Lorentzian Kubo-Toyabe function cannot be expressed in closed form, but numerical solutions are available. The characteristic feature of the weakly dynamic case is the exponential decay of the 1/3-signal whose depolarization rate is proportional to  $1/\tau$ . Raising the temperature further causes the spin fluctuation rate to increase rapidly. One first observes stretched exponential muon spin relaxation, later fast exponential relaxation (Eq. (2)).

### 3.4 Nuclear relaxation

As pointed out above, the local field  $B_\mu$  may possess a contribution generated by the nuclear magnetic dipole moments surrounding the stopped muon. This nuclear contribution is in general considerably weaker and can be neglected for ordered magnetic states, but not necessarily in the paramagnetic regime. In the present study, the main contribution comes from  $^{27}\text{Al}$  nuclear moments, but Mn and Co also carry nuclear moments which, however, are negligible in first approximation. For TF measurements the spectral shape is not much influenced by the nuclear contribution, the only effect is a small addition to the muon spin relaxation rate  $\lambda$ . In ZF spectra the combined muon spin relaxation by nuclear and atomic fields results in a different spectral shape than relaxation by atomic fields alone. The reason is the different dynamics of the atomic and nuclear magnetic moments. If the atomic and nuclear moments are not coupled, as is the case if the nuclear moments are on a non magnetic constituent (Al), the resulting (double relaxation) spectral function is the product of the atomic and the nuclear functions:

$$G_{dblrel}^{ZF}(t) = G_{atomic}^{ZF}(t) \cdot G_{nuclear}^{ZF}(t). \quad (6)$$

If the atomic moments are rapidly fluctuating, as is the case in a paramagnet, their spectral function is given by equation (2). The nuclear moments can usually be viewed as a static isotropic dense random spin system. In this case the spectral function is the Static Gaussian Kubo-Toyabe function (SGKT):

$$G_{SGKT}^{ZF}(t) = (2/3)(1 - \Delta_n^2 t^2) \exp(-\Delta_n^2 t^2/2) + (1/3) \quad (7)$$

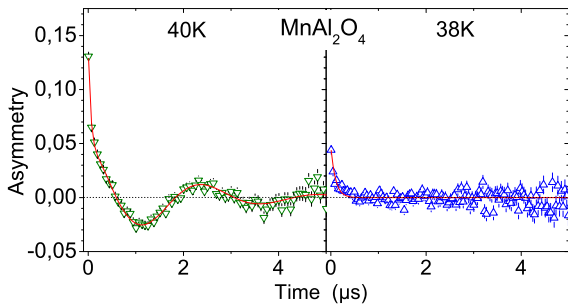


**Fig. 1.** (Color online) TF = 3 mT spectra of  $\text{MnAl}_2\text{O}_4$  above and below the magnetic transition point at 39 K. The spectrum at 40 K was fitted with the sum of a slowly and a fast exponentially damped oscillatory signal. At 38 K only a single fast exponentially decaying signal with reduced intensity was used.

where  $\Delta_n/\gamma_\mu$  is the *rms* nuclear field. In a longitudinal field  $G_{\text{SGKT}}^{LF}(t)$  has the characteristic property that depolarization is suppressed (i.e.  $G_{\text{SGKT}}^{LF}(t) \equiv 1$ ) if  $B_{\text{LF}} \geq 5\Delta_n/\gamma_\mu$ . The nuclear *rms* fields are typically less than 1 mT, hence  $B_{\text{LF}} = 5$  mT suffices to suppress the influence of nuclear relaxation. Since 5 mT does not affect the atomic relaxation rate it is common practice to investigate the behavior of paramagnetic relaxation in weak LF rather than in true ZF measurements. It is rewarding, however, to study at least at some key temperatures the nuclear relaxation as well by performing ZF measurements. For example, a possible onset of muon motion can be determined sensitively because the nuclear Gaussian Kubo-Toyabe function would then leave its static limit.

## 4 Results

In general we have recorded TF as well as ZF or LF spectra for the various compounds. TF data mainly serve the purpose to obtain a good value for the initial asymmetry  $A_0$ , and to determine the possible occurrence and location of a phase transition. Furthermore, in case the sample signal consists of several subspectra, it is usually easier to separate the different components in TF spectra. On the other hand, details of the magnetic properties are more precisely extracted from ZF or LF results. In TF measurements the magnetic field is applied transversely to the direction of flight of the muons resulting in beam bending. We kept  $B_{\text{TF}}$  low (3 mT) to ensure that the beam hits the sample practically under the same geometrical conditions as in ZF and LF measurements taken in the same series of data.

### 4.1 $\text{MnAl}_2\text{O}_4$

The TF = 3 mT spectra (examples are depicted in Fig. 1) show a distinct change in spectral shape between 38 K and 40 K signaling the occurrence of a magnetic phase transition. The transition temperature of 39 K agrees with

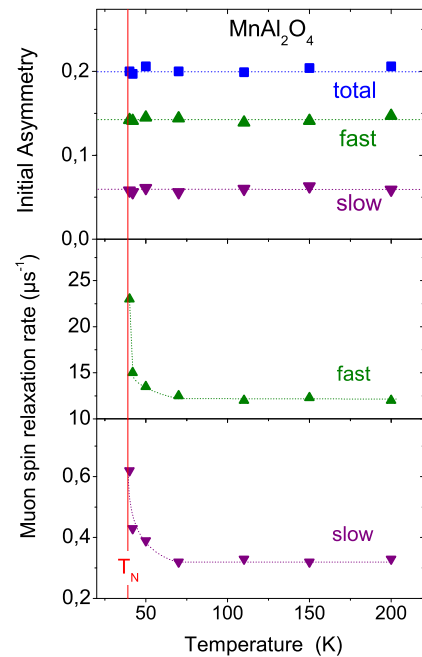


**Fig. 2.** (Color online) Temperature dependences of the initial asymmetries (upper panel) and of muon relaxation rates of the fast (center panel) and the slow (lower panel) subsignals for  $\text{MnAl}_2\text{O}_4$  in the paramagnetic regime. The dotted lines are guides to the eye.

$T_N$  obtained from susceptibility and neutron diffraction. It is sharply defined.

Above  $T_N$  the spectra consist of two subsignals, one slowly ( $\lambda_{\text{slow}}$ ) and the other fast relaxing ( $\lambda_{\text{fast}}$ ). The slow signal shows oscillations with the frequency corresponding to the applied field, as expected for a normal paramagnetic state. The other signal decays so rapidly that the oscillatory pattern cannot develop. The intensities of the two substates are temperature independent (see Fig. 2, upper panel). One finds  $A_{\text{total}} = A_{\text{fast}} + A_{\text{slow}} \approx 0.2$  and the ratio  $A_{\text{fast}}/A_{\text{total}} \approx 0.72$ . The asymmetries  $A_{\text{fast}}$  and  $A_{\text{slow}}$  are directly proportional to the volume fractions of the spin states producing the subsignals.

The ZF spectra in the paramagnetic range (an example is shown in Fig. 3a) need to be analyzed with the double relaxation formalism (Eqs. (6) and (7)). The nuclear relaxation parameter is small ( $\Delta_n = 0.1 \mu\text{s}^{-1}$ ) corresponding to  $B_{\text{rms}} = 0.12$  mT. This is a low value even for a nuclear dipole field. Probably the muon rests at some distance from the Al ions. The temperature dependences of the fast and slow muon spin relaxation rates in the paramagnetic regime of  $\text{MnAl}_2\text{O}_4$  are plotted in Figure 2.

The TF and ZF  $\mu\text{SR}$  data tell that above  $T_N$  two paramagnetic states coexist. Here slow muon relaxation means fast paramagnetic spin fluctuations (see Eq. (2)) which in turn indicate that the paramagnetic spins are only weakly coupled as expected for a *normal paramagnetic state*. The fast relaxation in the second subsignal is due to much slower paramagnetic spin fluctuations and thus reflects markedly stronger correlations between neighboring spins. We term this the *cooperative paramagnetic state*.

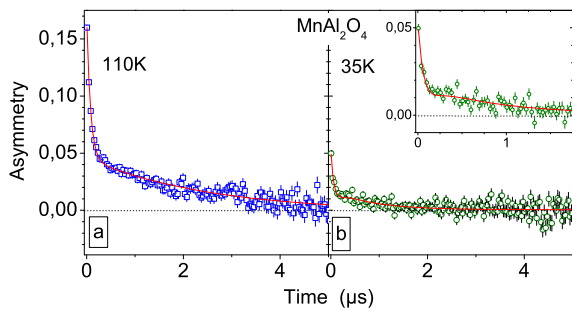


**Fig. 3.** (Color online) Typical ZF spectra of  $\text{MnAl}_2\text{O}_4$  above (a) and below  $T_N = 39\text{ K}$  (b). For  $T > T_N$  the spectral functions are atomic-nuclear double relaxation for both subspectra. For  $T < T_N$  the spectral function is the dynamic Lorentzian Kubo-Toyabe function. The inset shows the initial part of the spectrum in high time resolution.

The spins in both substates exhibit critical slowing down on approaching  $T_N$  from above (Fig. 2). Together with the shape of the temperature variation of the ordered moment seen in neutron diffraction, this proves the magnetic phase transition in  $\text{MnAl}_2\text{O}_4$  to be of second order.

Below  $T_N$  one can no longer distinguish two signals, neither in TF nor in ZF. The visible signal has a strongly reduced intensity. Its initial asymmetry corresponds to  $A_{\text{slow}}$  found for  $T > T_N$  and is also independent of temperature. The fact, that the intensity of the visible signal equals  $A_{\text{slow}}$  means that this spectrum reflects the properties of the magnetic state taken below  $T_N$  by the substate which behaved as a normal paramagnet above  $T_N$ . In this case a single signal fit is required which, however is not a simple exponential decay as can be seen from Figure 3b.

A satisfactory reproduction of spectral shape could be obtained using the dynamic Lorentzian Kubo-Toyabe function (DLKT) which is the  $\mu\text{SR}$  response of a spin-glass-like state in the dynamic region. A spin fluctuation rate of  $1/\tau \approx 5\text{ MHz}$  was found. The HWHM of the local field distribution  $a/\gamma_\mu$  is on the order of 30 mT, a value commonly experienced. Both, the HWHM and the spin fluctuation rate do not change on reducing the temperature down to 2 K. That means that complete spin freezing never takes place. Due to this feature of persistent spin dynamics on the one side, and the Kubo-Toyabe spectral shape on the other side, the spins below  $T_N$  must be considered to be in a glassy type state just above the critical glass temperature. This means, they form a spin liquid (SL) state having very slow spin dynamics (i.e. in the picture of a normal glass forming a highly viscous liquid). Yet, the total intensity  $A_{\text{total}}$  of the  $\mu\text{SR}$  spectra of any specific compound must be independent of temperature if the measurement geometry is maintained. Since below  $T_N$  part of the  $\mu\text{SR}$  response of  $\text{MnAl}_2\text{O}_4$  is not visible in the recorded spectra, it must be hidden in the initial dead time of the  $\mu\text{SR}$  spectrometer. Because the existence of an antiferromagnetically ordered state with transition temperature of  $\sim 40\text{ K}$  is definitely established by neutron diffraction, we are forced to conclude that the invisible signal of intensity  $A_{\text{fast}}$  is that of the long-range ordered state

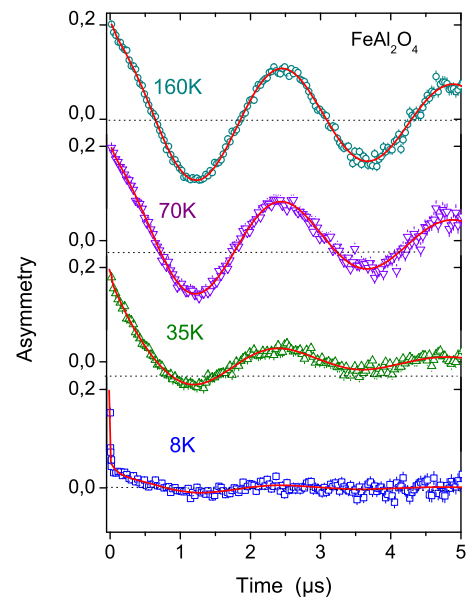


**Fig. 4.** (Color online) TF = 3 mT spectra of  $\text{FeAl}_2\text{O}_4$  at different temperatures. The spectra were fitted by the sum of a slowly and a fast relaxing oscillatory signal. The rapid decay of the fast relaxing signal prevents the appearance of an oscillatory pattern for this fraction.

whose  $\mu\text{SR}$  signal is described by equation (4). Vanishing in the spectrometer dead time means that both, the 2/3 and the 1/3 signal of equation (4) must damp out in 5 ns and this in turn requires that  $\lambda_{\text{trans}}$  and  $\lambda_{\text{long}}$  must exceed  $100\ \mu\text{s}^{-1}$ . We cannot draw any detailed conclusions on the properties of the long-range ordered state, except that it is formed out of the cooperative paramagnetic spin fraction and that, according to its high relaxation rates, large local spin disorder (on the scale of some atomic distances) exists in the antiferromagnetic spin lattice together with persistent fast spin fluctuations. The magnetic ground state of  $\text{MnAl}_2\text{O}_4$  then contains a long-range and a short-range ordered fraction. The volume fraction of the antiferromagnetic state  $A_{\text{fast}}/A_{\text{total}} = 0.72$  corresponds well to the ratio of observed to expected moment in neutron diffraction  $\mu_{\text{ord}}/\mu_{\text{spin}} = 3.7/5 = 0.74$ , thus providing an explanation for the measurement of a reduced ordered moment.

## 4.2 $\text{FeAl}_2\text{O}_4$

Also in this case, the TF = 3 mT, the ZF and the LF = 5 mT spectra all gave comparable results regarding the parameters of interest. The spectra consist also at all temperatures of two subsignals with different muon spin relaxation rates, but with their relative fractions being distinctly temperature dependent in contrast to the situation in  $\text{MnAl}_2\text{O}_4$ . Typical TF spectra are shown in Figure 4. The normalized intensity of the fast relaxing fraction and the relaxation rates of both fractions are plotted as a function of temperature in the left part of Figure 5. Analyzing the ZF spectra with the double relaxation formalism we find a similar nuclear mean field ( $\sim 0.13\text{ mT}$ ) as

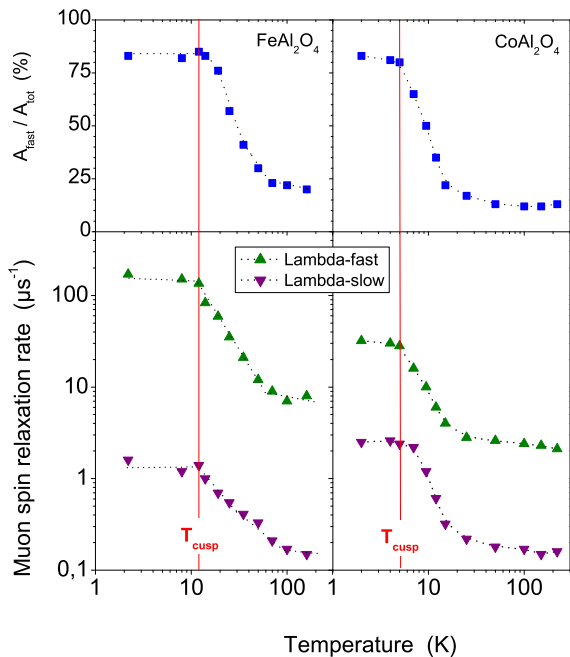


**Fig. 5.** (Color online) Temperature dependences of the normalized amplitude of the fast relaxing signal and of the fast and slow muon spin relaxation rates for  $\text{FeAl}_2\text{O}_4$  (left panels) and  $\text{CoAl}_2\text{O}_4$  (right panels). The dotted lines are guides to the eye.  $T_{\text{cusp}}$  is the cusp temperature seen in the susceptibility data. The statistical errors are equal or smaller than the size of the plot symbols.

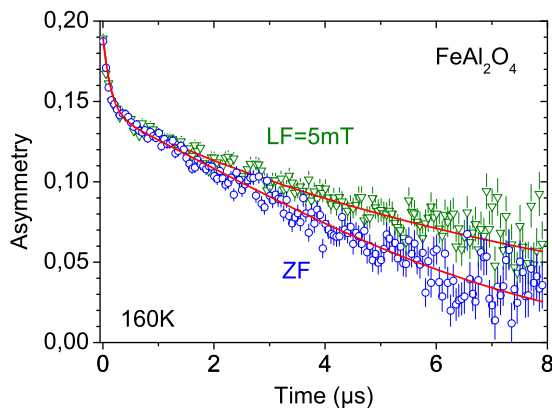


**Fig. 6.** (Color online) Comparison of the ZF and LF = 5 mT spectrum of  $\text{FeAl}_2\text{O}_4$  showing the suppression of nuclear relaxation by a weak longitudinal field. The solid lines are fits using the double relaxation formalism of equation (6).

in  $\text{MnAl}_2\text{O}_4$ . This weak nuclear relaxation can easily be suppressed by a small longitudinal field (5 mT) as demonstrated in the spectra shown in Figure 6.

A coexistence of normal and cooperative paramagnetism is present in  $\text{FeAl}_2\text{O}_4$  as well. In the high temperature limit the gross majority of spins ( $\sim 80\%$ ) is in the normal paramagnetic state. When reducing the temperature, the cooperative paramagnetic fraction increases, first slowly, then rapidly, reaching saturation ( $\sim 85\%$ ) at 12 K. This temperature corresponds to  $T_{\text{cusp}}$  in the suscep-

tibility data. Most important, a transition into long-range magnetic order does not take place in accordance with the lack of magnetic Bragg peaks in neutron diffraction data. The magnetic state below  $T_{\text{cusp}} = 12$  K is only short range ordered, yet it is not a spin glass with  $T_{\text{cusp}}$  being the glass transition temperature. If that were the case, its ZF  $\mu\text{SR}$  signature would be a static Lorentzian Kubo-Toyabe pattern. Furthermore, earlier low temperature specific heat data exhibited a  $T^2$  and not the linear temperature dependence expected for a spin glass [16]. It has been suggested [28] that a  $T^2$  dependence of the specific heat is an indicator for a spin liquid state. The presence of such a spin state also agrees with the observation of a liquid-like neutron structure factor [5]. In  $\text{MnAl}_2\text{O}_4$  the non ordered low temperature state manifests itself as a slowly dynamic Lorentzian Kubo-Toyabe pattern, whereas in  $\text{FeAl}_2\text{O}_4$  one observes an exponential decay. One should, however, remember that exponential relaxation is the fast fluctuation limit ( $1/\tau > \gamma_\mu B_{\text{HWHM}}$ ) of the dynamic Lorentzian Kubo-Toyabe function.

In the next section we compare some results for  $\text{CoAl}_2\text{O}_4$  with those of  $\text{FeAl}_2\text{O}_4$  leading to a spin fluctuation rate at  $T = 2$  K of  $1/\tau \approx 80$  MHz for the latter. The magnetic ground state of  $\text{FeAl}_2\text{O}_4$  thus consists of clearly dynamic short-range-correlated spins which we interpret as a spin liquid state well above a spin freezing temperature. Since the spin fluctuations are persistent below  $T_{\text{cusp}}$  no approach to spin freezing occurs. The spin liquid state coexists with a minute fraction of nearly free paramagnetic moments.

### 4.3 $\text{CoAl}_2\text{O}_4$

The results from analyzing the weak TF, ZF and weak LF spectra are in their basic appearances quite similar to those of  $\text{FeAl}_2\text{O}_4$  (see the right panels of Fig. 5). The influence of nuclear magnetism on the ZF spectra for  $T > T_{\text{cusp}}$  is slightly more pronounced in the Co compound. We find a mean nuclear field of 0.25 mT. The origin of this increase in field is not clear.

The main difference to  $\text{FeAl}_2\text{O}_4$  are distinctly smaller (roughly by an order of magnitude) values of the fast muon spin relaxation rate meaning (since we are outside long-range order) faster fluctuations of the cobalt moments. This is in agreement with the lower value of  $T_{\text{cusp}}$ . Noticeable is also that the change in slope of the curve  $A_{\text{fast}}(T)$  occurs around 15 K which corresponds to  $T/T_{\text{cusp}} \sim 3$  whereas in the iron spinel it occurs around 70 K or  $T/T_{\text{cusp}} \sim 6$ . With regard to the magnetic ground state of  $\text{CoAl}_2\text{O}_4$  we come to the same conclusions as in  $\text{FeAl}_2\text{O}_4$ , namely that a dynamic spin liquid state with persistent and even faster magnetic spin fluctuations is formed, coexisting with a minute residual fraction of paramagnetic spins.

We have further taken data in a strong longitudinal field ( $B_{\text{LF}} = 0.3$  T) at  $T = 2$  K, that is within the spin liquid state. It was found that under the applied LF pure exponential relaxation is still present with only a small reduction in rate. This is a clear indicator that the spins are in the fast fluctuation regime. There, the change in

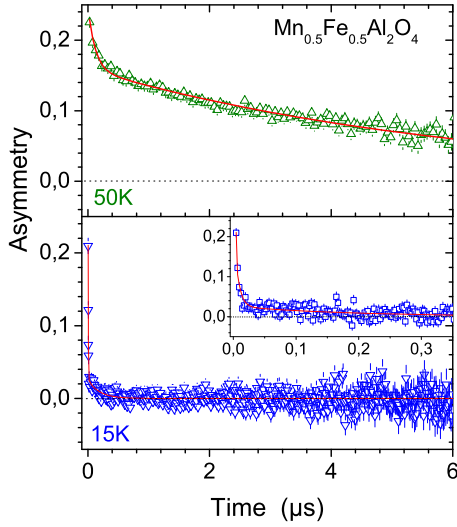


**Fig. 7.** (Color online) Typical LF = 5 mT spectra of  $\text{Mn}_{0.5}\text{Fe}_{0.5}\text{Al}_2\text{O}_4$  at high and low temperature. The least squares fit (solid lines) is for both spectra the sum of two exponentially relaxing subspectra. The inset at the lower panel shows the initial part of the spectrum in greater detail.

exponential relaxation rate with longitudinal field is given by [29]:

$$\frac{\lambda(B_{\text{LF}})}{\lambda(0)} = \frac{1}{1 + (\gamma_{\mu} B_{\text{LF}} \tau)^2}. \quad (8)$$

The measured ratio  $\lambda(0.3 \text{ T})/\lambda(0) = 19/24 \approx 0.8$  leads to  $1/\tau \approx 500 \text{ MHz}$ . The spin liquid state is indeed highly dynamic. If one further assumes that the width of the atomic field distribution is roughly the same in the spin liquid state of both compounds one estimates  $1/\tau$  to be about 80 MHz in  $\text{FeAl}_2\text{O}_4$  as mentioned before.

#### 4.4 $\text{Mn}_{0.5}\text{Fe}_{0.5}\text{Al}_2\text{O}_4$

Since  $\mu\text{SR}$  found substantial differences in the magnetic properties between  $\text{MnAl}_2\text{O}_4$  and  $\text{FeAl}_2\text{O}_4$ , it deemed useful to study the compound  $\text{Mn}_{0.5}\text{Fe}_{0.5}\text{Al}_2\text{O}_4$ . Measurements and data analysis were carried out as before. Figure 7 displays two characteristic LF = 5 mT spectra. As usual, two exponentially relaxing subsignals with notably different rates are present.

The results for  $\text{Mn}_{0.5}\text{Fe}_{0.5}\text{Al}_2\text{O}_4$  differ substantially from those of normal  $\text{MnAl}_2\text{O}_4$ . First, the relative fractions of the two signals are no longer temperature independent. Second, no sharp phase transition into a long-range ordered state takes place. The temperature dependence of the main spectral parameters plotted in Figure 8 indicates a sudden increase of muon relaxation rates between approximately 40 K and 20 K or, in other words, a rapid increase of spin-spin correlations. Interestingly, the onset of enhanced spin-spin correlations occurs at the same temperature where in  $\text{MnAl}_2\text{O}_4$  long-range order commences. In the same temperature range where the fast relaxation rate increases rapidly from 10 to 200  $\mu\text{s}^{-1}$ , the cooperative paramagnetic fraction rises from about 40% to nearly

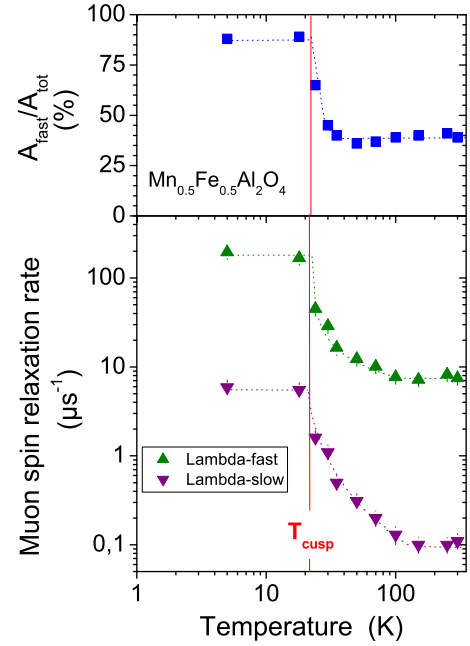


**Fig. 8.** (Color online) Temperature dependences of the fraction of the fast relaxing signal and of the fast and slow muon spin relaxation rates for  $\text{Mn}_{0.5}\text{Fe}_{0.5}\text{Al}_2\text{O}_4$ . The dotted lines are guides to the eye.

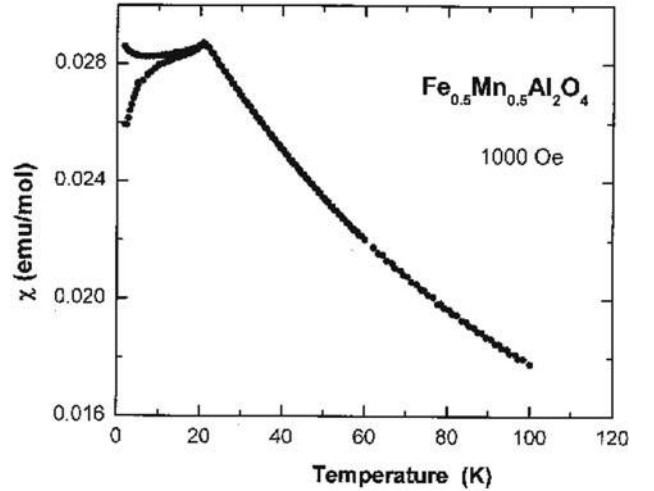


**Fig. 9.** Temperature dependences of the magnetic susceptibility in  $\text{Mn}_{0.5}\text{Fe}_{0.5}\text{Al}_2\text{O}_4$ . The two branches below  $T_{\text{cusp}} = 22 \text{ K}$  refer to field cooled and zero field cooled measurements.

90%. Having reached these values, the rate and the fraction are saturated as in  $\text{FeAl}_2\text{O}_4$  below  $T_{\text{cusp}}$ . The essential result is, the lower the temperature, the closer the magnetic behavior of  $\text{Mn}_{0.5}\text{Fe}_{0.5}\text{Al}_2\text{O}_4$  shifts toward that of  $\text{FeAl}_2\text{O}_4$ . In particular,  $\mu\text{SR}$  finds in  $\text{Mn}_{0.5}\text{Fe}_{0.5}\text{Al}_2\text{O}_4$  for its magnetic ground state a pure spin liquid state (except for the weak coexisting paramagnetic state) without any additional long-range ordered fraction.

The temperature dependence of the magnetic susceptibility in  $\text{Mn}_{0.5}\text{Fe}_{0.5}\text{Al}_2\text{O}_4$  measured recently in this context is depicted in Figure 9. It shows a behavior similar to that of  $\text{FeAl}_2\text{O}_4$  [16]. In particular, a cusp is seen at

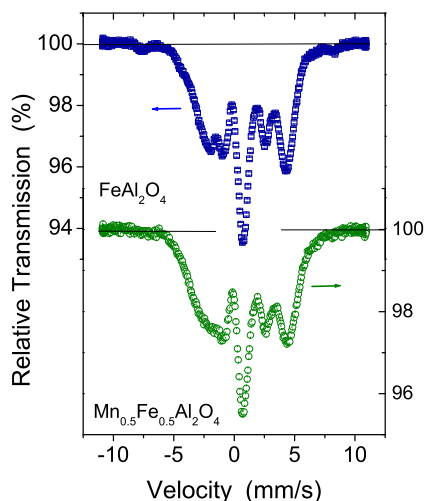


**Fig. 10.** (Color online) Comparison of the  $^{57}\text{Fe}$  Mössbauer spectra at 4.2 K of  $\text{FeAl}_2\text{O}_4$  and  $\text{Mn}_{0.5}\text{Fe}_{0.5}\text{Al}_2\text{O}_4$ .

22 K agreeing well with the temperature where the  $\mu\text{SR}$  spectra settle into their low temperature behavior.

The similarity in properties of the low temperature magnetic states of  $\text{Mn}_{0.5}\text{Fe}_{0.5}\text{Al}_2\text{O}_4$  and  $\text{FeAl}_2\text{O}_4$  is not only seen in their  $\mu\text{SR}$  and susceptibility data, but is also corroborated by their 4.2 K Mössbauer spectra (see Fig. 10). The two spectra are quite alike in their essential features and not typical for long-range order. Furthermore, the isomer shift indicates that the iron replacing the manganese is also in the  $2+$  state. Our spectrum of  $\text{FeAl}_2\text{O}_4$  is similar to that published earlier [18]. The results of that study have briefly been discussed in the introductory section.

The paramagnetic state coexisting with the spin liquid state below  $T_{\text{cusp}} = 22$  K is of even lower intensity than in  $\text{FeAl}_2\text{O}_4$ . One may add, at this point, that the detection of this coexisting paramagnetic state of very low intensity demonstrates the high sensitivity of  $\mu\text{SR}$  for different magnetic phases. Hence we can consider the sample to be free of contaminating foreign magnetic materials within the limit of a few percent.

From the high temperature slope of the inverse susceptibility one gets  $\Theta_{\text{CW}} = -126$  K for  $\text{Mn}_{0.5}\text{Fe}_{0.5}\text{Al}_2\text{O}_4$ , which in combination with  $T_{\text{M}} = T_{\text{cusp}} = 22$  K leads to a frustration parameter  $f \approx 6$ , a value which lies between those of  $\text{MnAl}_2\text{O}_4$  and  $\text{FeAl}_2\text{O}_4$ .

#### 4.5 $\text{Fe}_{1.4}\text{Al}_{1.6}\text{O}_4$

Inversion, i.e. A-B site exchange, is well documented in spinels. In order to evaluate the effects of inversion in  $\text{AAl}_2\text{O}_4$  we have studied a sample of  $\text{Fe}_{1.4}\text{Al}_{1.6}\text{O}_4$  possessing substantial inversion. Since, according to X-ray powder diffraction the material maintained the spinel crystal structure, one may safely assume that the excess Fe ions occupy the B-site together with the remaining Al ions. The compound should be viewed as a partially inverted spinel having all lattice sites occupied. At present we have no

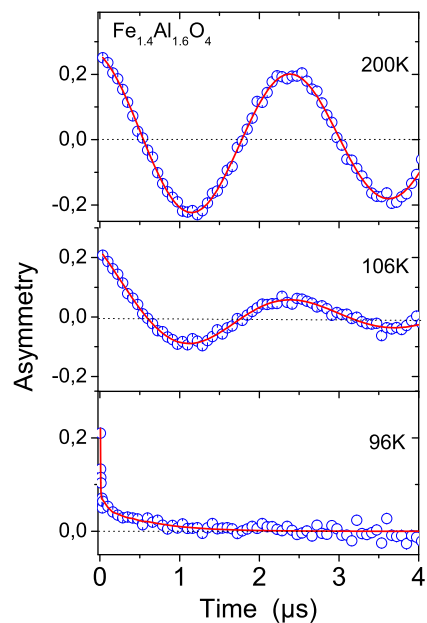


**Fig. 11.** (Color online) TF = 3 mT spectra of  $\text{Fe}_{1.4}\text{Al}_{1.6}\text{O}_4$  at 200 K, 106 K, and 96 K. The spectra at 200 K and 106 K were fitted with the sum of two exponentially damped oscillatory subspectra. The fast relaxing subspectrum is of very low intensity at 200 K. Note that the slowly relaxing subspectrum at 96 K shows no spin precession pattern (see text for explanation). The coarse fit of the 96 K spectrum shown here uses the sum of two exponential decaying subspectra. The more thorough treatment needed to obtain details of the spectral response is presented in Figure 13.

information whether the B-site ion distribution is random or whether a superstructure has formed.

Inspecting the  $\mu\text{SR}$  spectra (some examples are shown in Fig. 11) reveals a sudden change in spectral shape between 106 K and 96 K indicating the occurrence of a phase transition around 100 K. In contrast to the TF spectra of  $\text{FeAl}_2\text{O}_4$  below  $T_{\text{cusp}}$  (see, for example, Fig. 4, bottom panel) the TF spectra of  $\text{Fe}_{1.4}\text{Al}_{1.6}\text{O}_4$  below the transition (like the spectrum at 96 K in Fig. 11) show no oscillations with  $B_{\text{TF}}$  in the slowly relaxing subspectrum. This means that  $\text{Fe}_{1.4}\text{Al}_{1.6}\text{O}_4$  below 100 K is spontaneously magnetized which prevents an external field to enter the bulk of the material. Therefore, the transition around 100 K must lead into a long-range ordered state having a ferromagnetic component. These findings are fully supported by the magnetization data shown in Figure 12. From the reciprocal susceptibility one derives  $\Theta_{\text{CW}} = -176$  K. Together with  $T_{\text{N}} = 100$  K this leads to the low frustration parameter  $f \approx 1.8$ .

At high temperatures ( $T \gg T_{\text{N}}$ )  $\text{Fe}_{1.4}\text{Al}_{1.6}\text{O}_4$  is nearly completely in the normal paramagnetic state. The cooperative paramagnetic fraction grows rapidly in intensity on reducing the temperature toward  $T_{\text{N}}$  reaching about 90% at  $T_{\text{N}}$ , the residual 10% remain paramagnetic. It is the cooperative paramagnetic fraction which forms below  $T_{\text{N}}$  the long-range ordered magnetic state. Critical slowing down is observed when  $T_{\text{N}}$  is approached from above, indicating a second order transition.

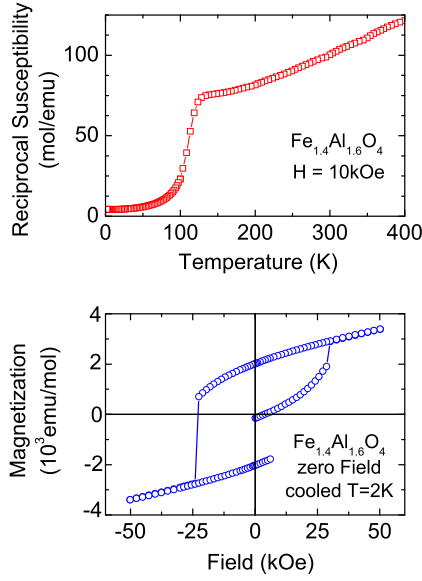


**Fig. 12.** (Color online) Bulk magnetic data of  $\text{Fe}_{1.4}\text{Al}_{1.6}\text{O}_4$ . Upper panel: temperature dependence of the reciprocal susceptibility ( $1/\chi$ ). Lower panel: magnetic hysteresis loop at 2 K.

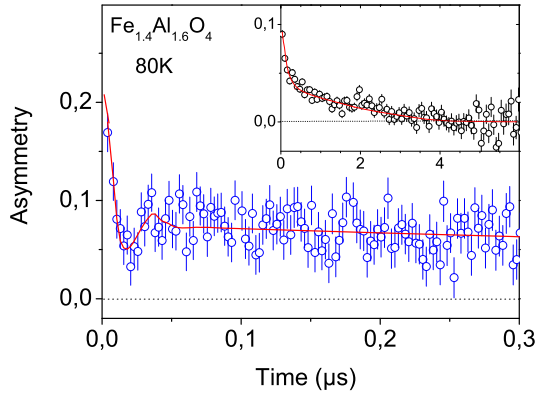


**Fig. 13.** (Color online) The main panel shows the early part of a typical spectrum of  $\text{Fe}_{1.4}\text{Al}_{1.6}\text{O}_4$  in the magnetically ordered regime in high time resolution. The fit uses the function given in equation (4). The inset shows the full spectral range in low time resolution where the spectral details seen at early times are averaged out.

Below  $T_N$  the fast subspectrum is expected to have the form of the  $\mu\text{SR}$  response of a long-range ordered magnet given in equation (4). To observe this behavior one has to analyze spectra taken in high resolution in the early time region. A characteristic case is depicted in Figure 13. The spontaneous spin precession pattern is heavily damped. The variation with temperature of the magnetic parameters for  $T < T_N$  derived from this analysis is shown in Figure 14. The interstitial field at the muon site behaves roughly like a Brillouin type magnetization curve. A fit to a particular model was not attempted since the detailed shape of  $B_\mu(T)$  is not well documented due to the limited structure in the  $\mu\text{SR}$  spectra. The magnitude of the saturation field  $B_\mu(0) = 0.43 \text{ T}$  is in the range often found in transition element magnets. The transverse relaxation

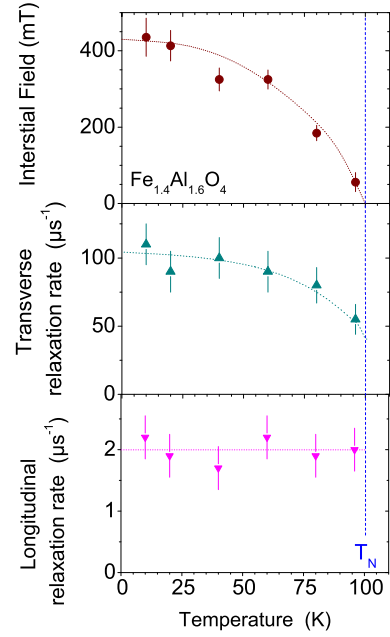


**Fig. 14.** (Color online) Temperature dependences of the interstitial field  $B_\mu$  and of the transverse and longitudinal muon spin relaxation rates in the magnetically ordered regime of  $\text{Fe}_{1.4}\text{Al}_{1.6}\text{O}_4$ . For details see text. The dotted lines are guides to the eye.

is large. It corresponds to a field distribution width of  $\sim 0.11 \text{ T}$  which is about 25% of the saturation field. The moment fluctuation rate in the ordered state deduced from the longitudinal relaxation is essentially temperature independent, while one expects it to approach zero in the low temperature limit.

Introducing iron on the B-site causes already at rather high temperature the formation of a reasonably well defined long-range ordered magnetic state with persistent spin fluctuations. A coexisting free paramagnetic fraction is only very weakly present.

## 5 Discussion

Our  $\mu\text{SR}$  results are best summarized in form of magnetic phase diagrams which are depicted in Figures 15 and 16. Not shown is the diagram for  $\text{CoAl}_2\text{O}_4$ , since in its basic appearance it is similar to that of  $\text{FeAl}_2\text{O}_4$ .

A general feature is the coexistence of two different magnetic phases in all compounds at all temperatures. In  $\mu\text{SR}$  studies one tends to introduce in such situations the existence of two muon stopping sites with different surroundings. This we exclude in the present case for the following reasons. First, the intensities of the two phases are different in the various compounds which all have the same crystal structure. Second, except for  $\text{MnAl}_2\text{O}_4$ , the intensity ratios are temperature dependent. If two muon stopping sites were involved, the muon would have to hop between the different sites on changing temperature. A muon hopping process would be visible in the nuclear relaxation pattern by a change of  $\Delta_n$  and by a move from

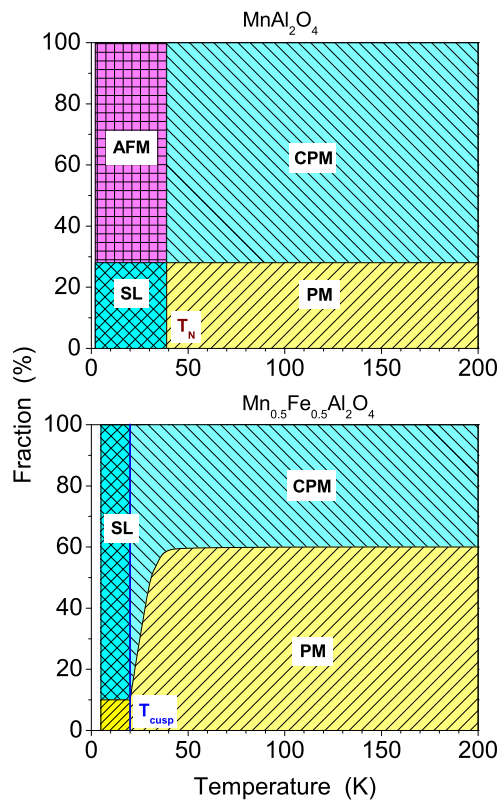


**Fig. 15.** (Color online) Magnetic phase diagram of  $\text{MnAl}_2\text{O}_4$  (Top) and  $\text{Mn}_{0.5}\text{Fe}_{0.5}\text{Al}_2\text{O}_4$  (Bottom). PM = normal paramagnet, CPM = cooperative paramagnet, SL = spin liquid (with slow dynamics in  $\text{MnAl}_2\text{O}_4$ , and faster dynamics in  $\text{Mn}_{0.5}\text{Fe}_{0.5}\text{Al}_2\text{O}_4$ ), AFM = antiferromagnet.

a static to a dynamic Gaussian Kubo-Toyabe function. None of these features are observed. Third, the change in intensity ratio with temperature is clearly coupled to the magnetic properties of the compound. For example, in  $\text{FeAl}_2\text{O}_4$  (and similarly in  $\text{CoAl}_2\text{O}_4$ ), the cooperative paramagnetic fraction increases rather rapidly when the characteristic magnetic temperature  $T_{\text{cusp}}$  is approached from above. Analogous behavior has been observed in other systems showing frustration by competing exchange, like the thio-spinels  $\text{FeSc}_2\text{S}_4$  [9] or  $\text{CuCrZrS}_4$  [30]. This suggests, that the coexistence of strongly and weakly spin correlated states is related to the presence of frustration by competing exchange. Although we have at this point no definite picture about its origin, one might envision that frustration breaks exchange paths and leads to some nearly free magnetic moments.

On the basis of the  $\mu\text{SR}$  spectra alone it is impossible to decide whether the two spin states are homogeneously distributed throughout the bulk or whether islets or even clusters are formed. Nevertheless, the spectral shape shows that the distribution of spin relaxation rates is bimodal, and not a single peaked broad distribution. If the latter were the case the decay of the muon spin polarization would follow a single stretched exponential instead of two exponential decays separated by their relaxation rates.

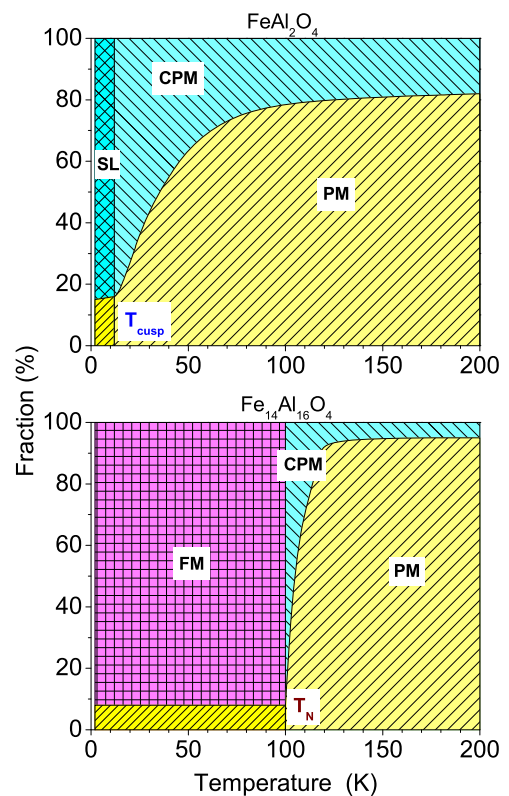


**Fig. 16.** (Color online) Magnetic phase diagram of  $\text{FeAl}_2\text{O}_4$  (Top) and  $\text{Fe}_{1.4}\text{Al}_{1.6}\text{O}_4$  (Bottom). PM = normal paramagnet, CPM = cooperative paramagnet, SL = spin liquid (fast dynamics), FM = ferrimagnet.

Fits with a single stretched exponential were tried, but proved incapable of reproducing the measured spectra.

Next we turn our attention to the nominal A-site spinels  $\text{AAl}_2\text{O}_4$ , especially how they transform from the the high temperature to the low temperature magnetic regimes. In  $\text{MnAl}_2\text{O}_4$ , the compound with the lowest frustration, the cooperative paramagnetic fraction which represents 72% of the spectrum at any temperature above  $T_N$ , enters at  $T_N = 39$  K into a long-range magnetically ordered state. The transition is of second order. It has been established by neutron diffraction that simple up-down collinear antiferromagnetic order exists [5]. Collinear spin order is particularly sensitive to suppression by frustration. Although such a state is formed, the existing frustration causes a high degree of local spin disorder (on the scale of lattice constants) and spin fluctuations (of at least 100 MHz) persisting for  $T \rightarrow 0$  in the antiferromagnetic spin lattice. These latter conclusions followed from the observation that the  $\mu\text{SR}$  signal of the ordered state has decayed within the dead time of the spectrometer ( $\sim 5$  ns), demanding large transversal and longitudinal relaxations. A second coexisting low temperature magnetic state is formed below  $T_N$  out of the normal paramagnetic fraction. It has been identified as a spin liquid state located close to, but still above the glass transition temperature. Since persistent slow spin fluctuations (5 MHz) are present, a freezing into a full glassy state is altogether excluded. One

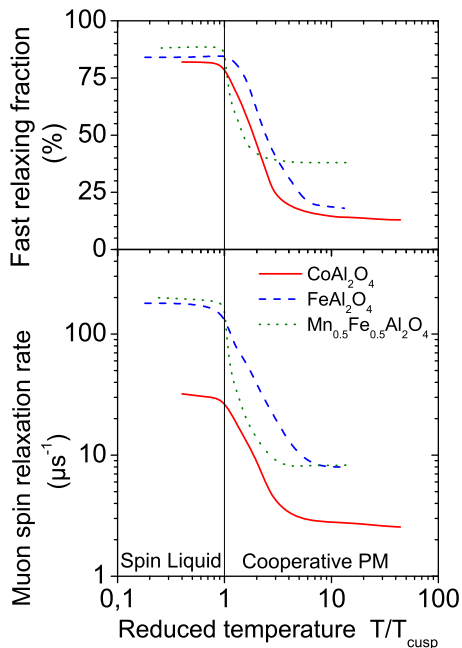


**Fig. 17.** (Color online) Comparison of the temperature dependences of the normalized intensity of the fast relaxing fraction and of the corresponding muon spin relaxation rate in  $\text{FeAl}_2\text{O}_4$ ,  $\text{CoAl}_2\text{O}_4$ , and  $\text{Mn}_{0.5}\text{Fe}_{0.5}\text{Al}_2\text{O}_4$  plotted as function of reduced temperature  $T/T_{\text{cusp}}$ . For a clearer picture only the smoothed lines connecting the data points are shown.

may suspect that the unusual coexistence of antiferromagnetic and spin liquid phases is an additional means of the spin system to allow collinear long-range order at least in part.

The much more strongly frustrated compounds  $\text{FeAl}_2\text{O}_4$  and  $\text{CoAl}_2\text{O}_4$  can no longer support any form of long-range magnetic order. Stronger frustration leads to enhanced fluctuations of the magnetic moments (see [3] and references therein) which are detrimental to long-range order. The muon spin relaxation rate  $\lambda_{\text{fast}}$  of the cooperative paramagnetic fraction is consistently lower in the more strongly frustrated  $\text{CoAl}_2\text{O}_4$  than in the weaker frustrated  $\text{FeAl}_2\text{O}_4$ , a fact clearly demonstrated in the lower panel of Figure 17 where these rates are plotted for the two compounds as function of reduced temperature  $T/T_{\text{cusp}}$ . This means (see Eq. (2)) that fluctuations of the magnetic moments are faster in  $\text{CoAl}_2\text{O}_4$  than in  $\text{FeAl}_2\text{O}_4$ .

The intensity of the cooperative paramagnetic fraction increases rapidly in both compounds when the temperature approaches  $T_{\text{cusp}}$  on cooling. It remains constant below  $T_{\text{cusp}}$  at about 85%. In  $\text{FeAl}_2\text{O}_4$  this increase begins at higher reduced temperature compared to  $\text{CoAl}_2\text{O}_4$  (see the top panel of Fig. 17). From the  $\mu\text{SR}$  spectral shape below  $T_{\text{cusp}}$  and in combination with specific heat and neutron data one concludes that the majority spin state must be viewed a highly dynamic spin liquid state. The persistence of spin fluctuations of about 80 MHz in  $\text{FeAl}_2\text{O}_4$  and 500 MHz in  $\text{CoAl}_2\text{O}_4$  keeps this state far above the freezing temperature even in the low temperature limit.

Little can be said about the small fraction of rapidly fluctuating spins coexisting with the spin liquid phase, except that these fluctuations are one (in  $\text{CoAl}_2\text{O}_4$ ) to two (in  $\text{FeAl}_2\text{O}_4$ ) orders of magnitudes faster than in the spin liquid state, putting them into the GHz range. Interestingly, also the shape of the temperature dependences of  $\lambda_{\text{fast}}$  and  $\lambda_{\text{slow}}$  are quite similar, indicating that an interaction exists between the two states. One could consider the minority state as a paramagnetic one with slightly enhanced spin-spin couplings when compared to the free paramagnetic state at high temperatures. In short, we find in  $\text{FeAl}_2\text{O}_4$  and  $\text{CoAl}_2\text{O}_4$  in the high temperature limit nearly pure normal paramagnetic and in the low temperature limit nearly pure spin liquid states. The characteristic temperature is  $T_{\text{cusp}}$  seen in susceptibility.

Moving next to the mixed spinel  $\text{Mn}_{0.5}\text{Fe}_{0.5}\text{Al}_2\text{O}_4$ , we find that the partial replacement of Mn by Fe in  $\text{MnAl}_2\text{O}_4$  changes the magnetic properties significantly. The relative intensities of the two paramagnetic phases are no longer temperature independent as they were in  $\text{MnAl}_2\text{O}_4$ . Furthermore, the cooperative fraction becomes more intense when decreasing the temperature, saturating at  $\sim 90\%$  in the low temperature limit. No magnetic phase transition into a long-range ordered state is found. Instead, the fluctuation rate in the cooperative paramagnetic fraction begins to slow down below 40 K and continues to be reduced rather steeply down to  $T_{\text{cusp}} = 22$  K where it levels off. According to its  $\mu\text{SR}$  parameters, the system is below 22 K in a spin liquid state similar to the low temperature situation in  $\text{FeAl}_2\text{O}_4$ .

Figure 17 also depicts for  $\text{Mn}_{0.5}\text{Fe}_{0.5}\text{Al}_2\text{O}_4$  the dependences on reduced temperature  $T/T_{\text{cusp}}$  of the intensity of the fast relaxing fraction and of its muon spin relaxation rate. Inspecting the top panel one notices that the high temperature limit is not a nearly pure normal paramagnetic state as in  $\text{FeAl}_2\text{O}_4$ , but, like in  $\text{MnAl}_2\text{O}_4$ , a substantial fraction of cooperative paramagnetism is present. The rise of the cooperative fraction starts later in the mixed spinel (at  $T/T_{\text{cusp}} \sim 2$ ) than in  $\text{FeAl}_2\text{O}_4$  (at  $T/T_{\text{cusp}} \sim 6$ ). Note that  $T/T_{\text{cusp}} \sim 2$  is near 40 K which is  $T_N$  for  $\text{MnAl}_2\text{O}_4$ . In the low temperature limit we see a behavior like in  $\text{FeAl}_2\text{O}_4$ , that is a nearly pure spin liquid phase coexisting with a minute paramagnetic fraction. In short, we find that some magnetic features of  $\text{Mn}_{0.5}\text{Fe}_{0.5}\text{Al}_2\text{O}_4$  remain reminiscent of  $\text{MnAl}_2\text{O}_4$ , but the overall behavior is close to that of  $\text{FeAl}_2\text{O}_4$ .

The changes in magnetic properties induced by replacing partially Al by Fe on the spinel B-site are dramatic in  $\text{Fe}_{1.4}\text{Al}_{1.6}\text{O}_4$ . Essentially all spins are in the normal paramagnetic state at high temperatures ( $T > 120$  K). Below 120 K, however, the intensity of the cooperative fraction increases suddenly and reaches rapidly 90% at 100 K where a transition into a long-range ordered spin state with a ferromagnetic component occurs. The negative Curie-Weiss temperature (see Fig. 12) then renders this state to be ferrimagnetic. Critical slowing down of the paramagnetic spin fluctuations on approaching  $T_N = 100$  K from above, together with the continuous decrease of  $B_\mu$  to zero when approaching  $T_N$  from below

shows the transition to be of second order. The Mössbauer spectrum at 4.2 K [32] indicates that one has  $\text{Fe}^{2+}$  on the A-site, as expected, and  $\text{Fe}^{3+}$  on the B-site.  $\text{Fe}^{3+}$  is a spin only ion like  $\text{Mn}^{2+}$  and furthermore the sequence of crystal field states is reversed in octahedral symmetry when compared to tetrahedral symmetry. This indeed causes different exchange behavior. The effect of Fe on the B-site then is clearly a substantial strengthening of the main magnetic exchange path. This is further demonstrated by the high value of  $\Theta_{\text{CW}}$  which exceeds that of the least frustrated pure A-site spinel  $\text{MnAl}_2\text{O}_4$ . One may visualize  $\text{Fe}_{1.4}\text{Al}_{1.6}\text{O}_4$  as a derivate of magnetite, a ferrimagnetic spinel where both A- and B-sites are occupied by Fe. That means we deal with a magnetite where more than half of the B-site Fe is replaced by non magnetic Al which reduces the Néel temperature from  $\sim 850$  K to  $\sim 100$  K.

Our  $\mu\text{SR}$  studies demonstrate that the A-site spinels of type  $\text{AAl}_2\text{O}_4$  are located in the border region between long-range and short-range magnetic order with frustration being the control parameter. The strength of frustration is conveniently expressed by the frustration parameter  $f$ . The interplay between long-range and short-range magnetic order as function of  $f$  is depicted in Figure 18, top panel. At very low values of  $f$  the whole material is an ordered magnet in the low temperature limit, neglecting the small fraction (about 10%) of coexisting paramagnetic spins. With rising  $f$  the relative volume fraction of long-range magnetic order decreases rapidly, the remaining fraction being taken up by the spin liquid phase. The limit where a long-range ordered fraction is present at all lies by  $f \approx 5$  in the  $\text{AAl}_2\text{O}_4$  system.

As was pointed out already, another characteristic feature of frustrated magnets are pronounced spin fluctuations which ease the effect of competing interactions on the magnetic ions. Therefore one expects the spin fluctuation rate to increase monotonically with stronger frustration. As shown in Figure 18, center panel, this is the case. The spin fluctuation rate as function of  $f$  follows a power law with a rather large exponent around 2. Since these data refer to the low temperature limit, they demonstrate that the spin fluctuations are persistent at low temperature, a feature observed in various frustrated magnets. Finally, we also plot the dependence on  $f$  of the critical temperature  $T_{\text{M}}$  (Néel temperature, cusp temperature etc.) in Figure 18, bottom panel. Clearly, the critical temperature and the spin fluctuation rate are coupled entities. Not unexpected, we find again a power law dependence, but the exponent is lower ( $-1.3$ ).

All data presented in Figure 18 firmly prove frustration to be the dominant factor controlling the magnetic properties of the A-site spinel series  $\text{AAl}_2\text{O}_4$ . Since frustration arises here from the different competing exchange interactions felt by the magnetic ions, variations in the strength of frustration means variations in the strength of the different exchange couplings. Because the lattice geometry is the same throughout the series, the main cause must be changes in electronic structure. The parameter

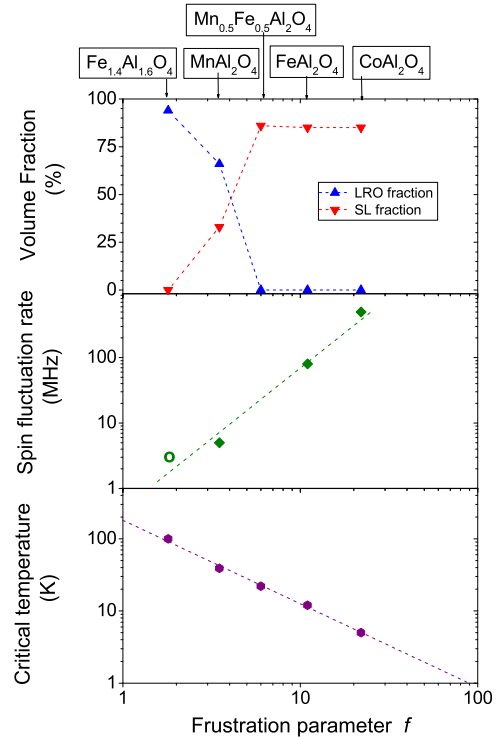


**Fig. 18.** (Color online) Influence of the frustration parameter on the volume fractions at  $T \rightarrow 0$  on the long-range ordered (LRO) and of the spin liquid (SL) fractions (top panel), on the fluctuation rate of the magnetic moments in the spin liquid state, except for  $\text{Fe}_{1.4}\text{Al}_{1.6}\text{O}_4$  (open circle) where the rate in the ferrimagnetic state is plotted (center panel), and on the critical temperature (either  $T_{\text{N}}$  or  $T_{\text{cusp}}$ ) (bottom panel). For  $\text{Mn}_{0.5}\text{Fe}_{0.5}\text{Al}_2\text{O}_4$  the spin fluctuation rate (center panel) cannot be properly evaluated. In the top panel, the dashed lines are guides to the eye, in the center and bottom panels the lines are power law fits. The deviation from 100% volume fraction in the top panel is due to the presence of a weak coexisting paramagnetic fraction (see the phase diagrams).

$f$  is a simple macroscopic quantity which gives no direct insight into the underlying microscopic situations.

Two relevant theoretical studies have appeared recently. The case of  $\text{CoAl}_2\text{O}_4$  is briefly mentioned in the treatment of frustrated diamond lattice antiferromagnets [3]. On the basis of a slightly simplified model containing only the two exchange paths  $J$  (nearest neighbors) and  $J'$  (next nearest neighbors) bond frustration is introduced by varying the ratio  $J'/J$ . Monte Carlo simulations reveal that the magnetic properties depend sensitively on the ratio  $J'/J$ . In the region  $0 \leq J'/J \leq 0.125$  the spin coupling is Néel-like with the Néel temperature rapidly reducing as  $J'/J = 0.125$  is approached. Above the critical ratio a spiral spin liquid phase is established in which the direction of the wave vector (determined from the position of the minima of the free energy within the Brillouin zone) depends on the value of  $J'/J$ . Specific spirals are entropically stabilized (order by disorder [31]) leading to complex non-linear magnetic order at lowest temperatures. However, the details of the ground state sensitively

depend on any additional interaction such as  $J''$ . It is argued [3] specifically, that the loss of long-range magnetic order in  $\text{CoAl}_2\text{O}_4$  as compared to  $\text{MnAl}_2\text{O}_4$  is achieved by shifting  $J'/J$  into the critical region slightly above 0.125.

## 6 Conclusions

The present  $\mu\text{SR}$  study reveals the magnetic properties of the A-site spinels  $\text{AAl}_2\text{O}_4$  to be prominently determined by their degree of frustration. The results on the various magnetic states formed are summarized in magnetic phase diagrams.

Above a critical magnetic temperature  $T_M$ , all compounds show a bimodal distribution of spin fluctuations. It is suggested that this duality is an outcome of the materials being shifted below the percolation limit. Below  $T_M$  the system enters either into a long-range ordered or a spin liquid state or a combination of both. A weak paramagnetic fraction usually remains present.

The nature of the magnetic ground state is determined by the value of the frustration parameter  $f = \Theta_{\text{CW}}/T_M$ . At very low values of  $f$  long-range order is present. At intermediate values a coexistence of long-range ordered and spin liquid states is observed. For  $f > 5$  long-range order is no longer possible, the system enters the spin liquid state in the low temperature limit. A general feature of all cases are spin fluctuations persisting for  $T \rightarrow 0$  and whose frequency becomes larger with increasing frustration. In addition, in the long-range ordered states considerable local spin disorder is present.

The experiments were carried out using the  $\mu\text{SR}$  spectrometers DOLLY and GPS at the Swiss Muon Source, Paul Scherrer Institute (PSI), Villigen-AG, Switzerland. We are indebted to H. Luetgens and R. Scheuermann for continuous support during the experiments. The work was supported in part by the Deutsche Forschungsgemeinschaft via TRR88/Augsburg-Munich.

## References

1. W. Schiessl, W. Potzel, H. Karzel, M. Steiner, G.M. Kalvius, A. Martin, M.K. Krause, I. Halevy, J. Gal, W. Schäfer, G. Will, M. Hillberg, R. Wäppling, Phys. Rev. B **53**, 9143 (1996)
2. P.W. Anderson, Phys. Rev. **102**, 1008 (1956)
3. D. Bergman, J. Alicea, E. Gull, S. Trebst, L. Balents, Nat. Phys. **3**, 487 (2007)
4. V. Fritsch, J. Hemberger, N. Büttgen, E.-W. Scheidt, H.-A. Krug von Nidda, A. Loidl, V. Tsurkan, Phys. Rev. Lett. **92**, 116401 (2004)
5. A. Krimmel, V. Tsurkan, D. Sheptyakov, A. Loidl, Physica B **378–380**, 583 (2006)
6. N. Büttgen, J. Hemberger, V. Fritsch, A. Krimmel, M. Mücksch, H.-A. Krug von Nidda, P. Lunkenheimer, R. Fichtl, V. Tsurkan, A. Loidl, New J. Phys. **6**, 191 (2004)
7. A. Krimmel, M. Mücksch, V. Tsurkan, M.M. Koza, H. Mutka, A. Loidl, Phys. Rev. Lett. **94**, 237402 (2005)
8. A. Krimmel, M. Mücksch, V. Tsurkan, M.M. Koza, H. Mutka, C. Ritter, D. Sheptyakov, S. Horn, A. Loidl, Phys. Rev. B **73**, 014443 (2006)
9. G.M. Kalvius, O. Hartmann, D.R. Noakes, F.E. Wagner, R. Wäppling, U. Zimmermann, Ch. Baines, A. Krimmel, V. Tsurkan, A. Loidl, Physica B **378–380**, 592 (2006)
10. G. Chen, L. Balents, A.P. Schnyder, Phys. Rev. Lett. **102**, 096406 (2009)
11. A.P. Ramirez, in *Handbook of Magnetic Materials*, edited by K.J.H. Buschow (Elsevier Science, Amsterdam, 2001), Vol. 13, p. 423
12. J.E. Greedan, J. Mater. Chem. **11**, 37 (2001)
13. A. Yaouanc, P. Dalmas de Reotier, P. Bonville, J.A. Hodges, P.C.M. Gubbens, C.T. Kaiser, S. Sakarya, Physica B **326**, 456 (2003)
14. G.M. Kalvius, D. Noakes, R. Wäppling, G. Grosse, W. Schäfer, W. Kockelmann, J.K. Yakinthos, P.A. Kotsanides, Physica B **326**, 465 (2003)
15. G.M. Luke, A. Keren, K. Kojima, L.P. Le, W.D. Wu, U.J. Uemura, G.M. Kalvius, A. Kratzer, G. Nakamoto, T. Takabatake, M. Ishikawa, Physica B **206**, 207, 222 (1995)
16. N. Tristan, J. Hemberger, A. Krimmel, H.-A. Krug von Nidda, V. Tsurkan, A. Loidl, Phys. Rev. B **72**, 174404 (2005)
17. A. Krimmel, H. Mutka, M.M. Koza, V. Tsurkan, A. Loidl, Phys. Rev. B **79**, 134406 (2009)
18. J.L. Dormann, M. Seqqat, D. Fiorani, M. Nogues, J.L. Soubeyroux, S.G. Bhargava, P. Renaudin, Hyperfine Int. **54**, 503 (1990)
19. G.M. Kalvius, A. Krimmel, O. Hartmann, F.J. Litterst, R. Wäppling, V. Tsurkan, A. Loidl, Physica B **404**, 660 (2009)
20. D.J. Arsenau, B. Hitti, S.R. Kreitzmann, E. Whidden, Hyperfine Int. **106**, 277 (1997)
21. G.M. Kalvius, D.R. Noakes, O. Hartmann, in *Handbook on the Physics and Chemistry of Rare Earth*, edited by K.A. Gschneidner Jr., L. Eyring, G.H. Lander (Elsevier Science, Amsterdam, 2001), Vol. 32, p. 55
22. *Muon Science*, edited by S.L. Lee, S.H. Kilcoyne, R. Cywinski (Institute of Physics, London, 1999)
23. E.B. Karlsson, *Solid State Phenomena As Seen By Muons, Protons and Excited Nuclei* (Clarendon Press, Oxford, 1995)
24. A. Schenck, *Muon Spin Rotation Spectroscopy* (Adam Hilger, Bristol, 1985)
25. O. Hartmann, E. Karlsson, R. Wäppling, J. Chappert, A. Yaouanc, L. Asch, G.M. Kalvius, J. Physics F: Metal Physics **16**, 1593 (1986)
26. R. Kubo, Hyperfine Int. **8**, 731 (1981)
27. Y.I. Uemura, T. Yamazaki, D.R. Harshmann, M. Semba, E.J. Ansaldo, Phys. Rev. B **31**, 546 (1985)
28. D. Zkou, C.R. Wiebe, Y.J. Yo, L. Balicus, Y. Takano, M.J. Case, Y. Qiu, J.R.D. Copley, J.S. Gardner, arXiv:cond-mat/0808 2819
29. C.P. Slichter, *The Principle of Magnetic Resonance* (Springer, Berlin, New York, 1976)
30. H.S. Suzuki, T. Furubayashi, Y. Kawashima, S. Nagata, T. Suzuki, T. Kawamata, I. Watanabe, T. Matsuzaki, A. Amato, Physica B **404**, 649 (2009)
31. J. Villain, R. Bidaux, J.P. Carton, R. Conte, J. Phys. **41**, 1263 (1980)
32. F.J. Litterst, F.E. Wagner, G.M. Kalvius, A. Krimmel, V. Tsurkan, A. Loidl (in preparation)